Microwave-Assisted Thermoelectricity in *S-I-S′* Tunnel Junctions

A. Hijano,[1,2,*] F.S. Bergeret,[1,3,†] F. Giazotto,[4,‡] and A. Braggio[4,§]

[1] *Centro de Física de Materiales (CFM-MPC), Centro Mixto CSIC-UPV/EHU, Donostia-San Sebastián 20018, Spain*

[2] *Department of Condensed Matter Physics, University of the Basque Country UPV/EHU, Bilbao 48080, Spain*

[3] *Donostia International Physics Center (DIPC), Donostia-San Sebastián 20018, Spain*

[4] *NEST Istituto Nanoscienze-CNR and Scuola Normale Superiore, Pisa 56127, Italy*

(Received 8 November 2022; revised 31 January 2023; accepted 15 March 2023; published 7 April 2023)

Asymmetric superconducting tunnel junctions with gaps $\Delta_1 > \Delta_2$ have been proven to show a peculiar nonlinear bipolar thermoelectric effect. This arises due to the spontaneous breaking of electron-hole symmetry in the system, and it is maximized at the matching-peak bias $|V| = V_p = (\Delta_1 - \Delta_2)/e$. In this paper, we investigate the interplay of photon-assisted tunneling (PAT) and bipolar thermoelectric generation. In particular, we show how thermoelectricity, at the matching peak, is supported by photon absorption and emission processes at the frequency-shifted sidebands $V = \pm V_p + n\hbar\omega$, $n \in \mathbb{Z}$. This represents a sort of *microwave-assisted thermoelectricity*. We show the existence of multiple stable solutions, being associated with different photon sidebands, when a load is connected to the junction. Finally, we discuss how the nonlinear cooling effects are modified by the PAT. The proposed device can detect millimeter-wavelength signals by converting a temperature gradient into a thermoelectric current or voltage.

DOI: 10.1103/PhysRevApplied.19.044024

I. INTRODUCTION

Hybrid superconducting systems with explicit broken particle-hole symmetry show unipolar thermoelectricity [1–9]. The particle-hole symmetry around the Fermi surface of Bardeen-Cooper-Schrieffer (BCS) superconductors can be broken, for instance, in superconductor/ferromagnet hybrid structures. The magnetic proximity effect in a thin superconductor-ferromagnetic insulator bilayer causes an almost homogeneous spin splitting of the density of states (DOS) [10]. If the electronic transport is spin-polarized, for example via a tunneling spin filter [11–14], the DOS contribution of one spin component becomes predominant over the other one, leading to an effective particle-hole symmetry breaking [4].

It has recently been theoretically [15–17] and experimentally [18,19] shown that superconducting tunnel junctions, where the Josephson coupling is properly suppressed, develop a large thermoelectric effect if the electrode with the larger gap has a higher temperature. In contrast to systems with magnetic proximity effect, in superconducting tunnel junctions the electron-hole symmetry is broken by the combination of a sufficiently strong thermal gradient and a monotonically decreasing DOS, which induces spontaneous voltage polarization. The resulting thermoelectricity is *bipolar* and strongly nonlinear.

We focus here on photon-assisted tunneling (PAT), which has been extensively studied in the dissipative regime [20–30]. However, the influence of PAT on the recently observed bipolar thermoelectricity is still unexplored. In this work, we address microwave-assisted thermoelectricity by investigating the interplay between PAT and bipolar thermoelectricity in a superconductor-insulator-superconductor (*S-I-S′*) tunnel junction. This kind of tunnel junction normally works at very low temperatures in order to preserve the superconductivity. It is worth noting that thermoelectricity at these temperatures is very strong [18] due to the nonlinearity of the effect. The obtained results show intriguing perspectives for application as millimeter-wavelength signal detectors [7], flux-controlled high-frequency oscillators [17], controlled generators [16], superconducting qubits [31–35], quantum sensors [36,37], and, more broadly, in the emergent field of superconducting quantum technologies.

This paper is organized as follows: In Sec. II we present the basic equations describing the dc and ac tunneling charge and heat currents through a tunnel junction. In Sec. III we numerically obtain the $I(V)$ characteristic curves and study the thermoelectric power output. Finally,

*alberto.hijano@ehu.eus
†fs.bergeret@csic.es
‡francesco.giazotto@sns.it
§alessandro.braggio@nano.cnr.it

we study the impact of the ac voltage source on the cooling power of the junction. We summarize the results in Sec. IV.

II. THE MODEL

We consider an S-I-S' tunnel junction where each superconducting electrode is kept in thermal equilibrium; see Fig. 1(a). The gap of the left superconductor (S_1) is considered to be higher than that of the right superconductor (S_2), $\Delta_1 > \Delta_2$. This can be done by using different superconducting materials for each electrode or by taking advantage of the inverse proximity effect by attaching a normal layer to the right superconductor, which effectively suppresses the gap [18]. The asymmetry parameter $r = \Delta_{0,2}/\Delta_{0,1} < 1$ quantifies the asymmetry between the two terminals, where $\Delta_{0,\alpha}$ is the zero-temperature gap of electrode α. If the electrodes are powered by a constant voltage source V, the chemical potential of the electrodes are shifted by $\mu_1 - \mu_2 = -eV$.

The tunneling current between the two superconductors has three contributions: the quasiparticle current, the Cooper-pair current, and the interference current, which gives the interference contribution associated with breaking and recombination processes of Cooper pairs in different electrodes [38–41]. The latter two contributions stem from the Josephson coupling, and they depend on the phase difference between the superconductors. At finite bias, those terms oscillate between positive and negative values, and might be detrimental to a stable thermoelectric effect [17]. Therefore, we assume that the Josephson coupling is sufficiently weak [18,42–44], and neglect those terms, such that we consider only the quasiparticle current, which is phase-independent. The Josephson current can also be suppressed by applying a suitable in-plane magnetic field or by applying a small out-of-plane magnetic field in a superconducting quantum interference device (SQUID) as in [18,19].

The dc tunneling quasiparticle charge I_α and heat $\dot{Q}_\alpha$ currents flowing out from electrode $\alpha = 1, 2$ are

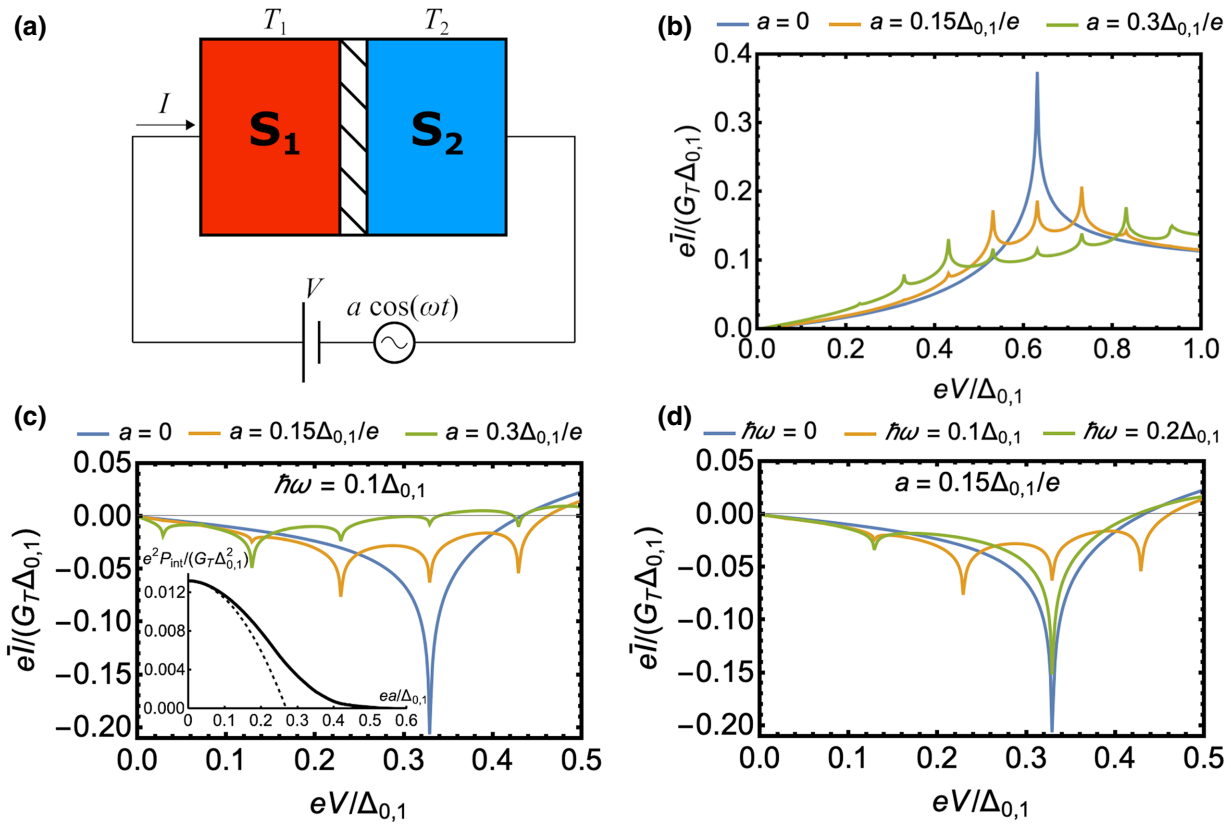

FIG. 1. (a) Simple circuit scheme of the photon-assisted bipolar thermoelectricity. The two superconductors have a different gap $\Delta_1 > \Delta_2$ and are subject to a temperature difference $T_1 > T_2$. The S-I-S' junction is powered by a dc and an ac voltage source. (b) Equilibrium $\bar{I}(V)$ curves for a finite ac voltage with $\hbar\omega = 0.1\Delta_{0,1}$ and different amplitudes a. (c,d) Time-averaged quasiparticle current $\bar{I}(V)$ dependence on the amplitude (c) and angular frequency (d) of the ac field. The inset in panel (c) shows the integrated thermoelectric power as a function of a (solid line) and the behavior predicted in the small-signal limit (dashed line). The temperatures are $T_1 = T_2 = 0.4T_{c,1}$ in panel (b), and $T_1 = 0.7T_{c,1}$ and $T_2 = 0$ for panels (c) and (d).

given by

$$\begin{pmatrix} I_\alpha \\ \dot{Q}_\alpha \end{pmatrix} = \frac{G_T}{e^2}\int dE \begin{pmatrix} -e \\ E-\mu_\alpha \end{pmatrix} N_\alpha(E-\mu_\alpha)N_{\bar{\alpha}}(E-\mu_{\bar{\alpha}}) \times (f_\alpha(E-\mu_\alpha) - f_{\bar{\alpha}}(E-\mu_{\bar{\alpha}})), \quad (1)$$

with $\bar{\alpha}$ the opposite side with respect to α. Here, $-e$ is the electron charge, G_T is the conductance of the junction, and $f_\alpha(E) = [\exp(E/k_B T_\alpha)+1]^{-1}$ is the α-lead Fermi-Dirac distribution. The BCS DOS is given by $N_\alpha(E) = \mathrm{Re}\{-i(E+i\Gamma_\alpha)/\sqrt{\Delta_\alpha^2-(E+i\Gamma_\alpha)^2}\}$, where Γ_α is the Dynes parameter [45], describing inelastic processes. The Dynes parameter accounts for the broadening of the BCS coherent peaks at $E=\pm\Delta$ in the DOS. In the calculations below, we set $\Gamma_1=\Gamma_2=10^{-4}\Delta_{0,1}$, which is a reasonable value typically found in experiments with high-quality tunnel junctions [46–49].

From Eq. (1), one can easily check that the S-I-S' is a reciprocal electric device. Indeed, the DOS of the superconducting electrodes is electron-hole symmetric, so that the quasiparticle charge current in the junction is odd in voltage $I(-V)=-I(V)$, where we focus here on the current flowing out of the left electrode, $I\equiv I_1$. Moreover, due to energy conservation, $\dot{Q}_1+\dot{Q}_2-\dot{W}=0$, where $\dot{W}=-VI$ describes the electric power generated (dissipated) for $\dot{W}>0$ ($\dot{W}<0$) by the junction. Here we use the active sign convention by considering the electrical work done by the junction over its surroundings as positive. At the equilibrium $T_1=T_2$, the junction is dissipative ($IV>0$). When the temperature of the left electrode, with a bigger gap, is higher than that on the right electrode, $T_1 \gtrsim T_2/r$, it is possible to generate bipolar thermoelectricity [15,18] with the current I flowing against the bias ($IV<0$). This occurs at subgap voltages $e|V| \lesssim \Delta_1+\Delta_2$ [15–17]. Furthermore, from the negative differential conductance at $V\approx 0$, the thermocurrent grows to a maximum around the matching peak $eV_p=\Delta_1-\Delta_2$, and for $e|V|\gtrsim\Delta_1+\Delta_2$ it again becomes dissipative. In an open-circuit configuration, a thermoelectric Seebeck voltage $\pm V_S$ is induced, for which $I(\pm V_S)=0$. The double sign of the Seebeck voltage reflects the *bipolarity* of the thermoelectric effect, which is a consequence of the reciprocity of the device.

If an ac source is included in addition to the dc voltage, $V(t)=V+a\cos(\omega t)$, for instance by placing the junction in a microwave field, the average current is no longer simply given by Eq. (1). The time-averaged dc tunnel (charge and heat) currents $\bar{I}=(1/T)\int_0^T dt\, I(t)$ and $\bar{\dot{Q}}=(1/T)\int_0^T dt\,\dot{Q}(t)$ take the form [20,30,50]

$$\begin{pmatrix} \bar{I} \\ \bar{\dot{Q}} \end{pmatrix} = \sum_{n=-\infty}^{\infty} J_n^2\left(\frac{ea}{\hbar\omega}\right)\begin{pmatrix} I(V-n\hbar\omega/e) \\ \dot{Q}(V-n\hbar\omega/e) \end{pmatrix}, \quad (2)$$

where $T=2\pi/\omega$ is the period of the ac voltage. This is the standard result for PAT, where $J_n(x)$ is the nth Bessel function of the first kind. In Eq. (2) we assume that the frequency of the ac voltage is small enough so that it modulates the potential energy of the quasiparticles adiabatically [25,51,52]. In this approximation, the ac frequency is necessarily bounded by the plasma frequency of the two electrodes and the driving frequency needs to be $\hbar\omega<2\Delta$, in order to neglect high-order processes in the current due to the direct breaking of Cooper pairs due to photon absorption. At the same time, we will mainly focus on quite small amplitudes of the voltage oscillations, $ea\ll\Delta$, as we will explain in Sec. III, since high amplitudes are detrimental for the thermoelectric effect restoring the usual dissipative behavior at high energies. Finally, the averaged current $\bar{I}$ is also reciprocal, $\bar{I}(-V)=-\bar{I}(V)$, due to the reciprocity of the junction $I(V)$. For this reason, in the following, we show only results for positive biases.

III. RESULTS

In Fig. 1(b) we show the $\bar{I}(V)$ characteristic curve for the equilibrium case $T_1=T_2=0.4T_{c,1}$ in the presence of PAT with $\hbar\omega=0.1\Delta_{0,1}$ for different amplitudes. As expected for equilibrium temperatures, the junction has only a dissipative behavior and the PAT introduces different sidebands near the matching peak V_p. Indeed, if the frequency $\hbar\omega/e$ of the ac voltage is larger than the width of the matching peak and the amplitude a is not too high (see later), we expect to see a weighted replication of the dc characteristics displaced in voltage in the sidebands. According to Eq. (2), one easily finds the position of the matching peak sidebands at $eV=eV_p+n\hbar\omega$, $n\in\mathbb{Z}$.

In Figs. 1(c) and 1(d) we show the $\bar{I}(V)$ characteristics when the junction is subject to a temperature difference $T_1=0.7T_{c,1}$ and $T_2=0$, with $T_{c,\alpha}$ the critical temperatures of the electrodes. The temperature difference of the electrodes has been chosen in order to maximize the thermoelectric effect, as previously stated [15]. Figures 1(c) and 1(d) show the effect of a and ω on $\bar{I}(V)$, respectively. For $a=0$ or $\omega=0$ (blue line), the voltage source has no ac component, so the electric current displays the conventional behavior for a single thermoelectric peak centered at $eV_p=\Delta_1-\Delta_2$. The sharpness of the thermoelectric peak depends on the phenomenological Dynes parameter, with lower Γ favoring sharper peaks.

As expected from Eq. (2), for a finite ac voltage source, the quasiparticle current presents multiple thermoelectric peaks which are separated periodically in voltage. As the value of a increases, the height of the main thermoelectric peak decreases in absolute value while the sidebands increase in size. Clearly, at fixed ω, by changing the amplitude a, the weights given by the Bessel functions change such that the height of the sideband peaks change correspondingly. Physically, for $V>0$, the sideband thermoelectric peaks in the averaged current correspond to

processes where photons are absorbed (emitted), respectively, for $n < 0$ ($n > 0$) to support thermoelectricity at the sideband voltages. Note that the signature of the thermoelectric peak corresponding to the sidebands can also be found in the dissipative regime as a dip of the $\bar{I}(V)$ characteristics [see the dip at $eV/\Delta_{0,1} \approx 0.45$ of the green line in Fig. 1(c)]. All sidebands do not necessarily become thermoelectric, being weighted by a different Bessel function and mixing different channels in the thermoelectric and dissipative regimes. In general, the $I(V)$ characteristic at sufficiently high voltages remains in the dissipative regime.

In other words, the ac source seems to redistribute the thermoelectric power to different sidebands. This can be better quantified by looking at the integrated thermoelectric power, defined as

$$P_{\text{int}} = -\int_0^{V_S} dV\bar{I}(V), \tag{3}$$

which decreases with increasing a [see inset of Fig. 1(c)], and remains almost constant under variations of ω (not shown). The dashed line in the inset corresponds to the power given in the small-signal limit. Indeed, when $x = (ea/\hbar\omega) \ll 1$, the variation of the averaged current may be obtained by expanding the Bessel functions to the lowest order $J_0(x) \approx 1 - x^2/4$ and $J_{\pm n}(x) \approx (\pm x/2)^n/n!$ in Eq. (2), and retaining only x^2 terms; one finds the current variation $\Delta\bar{I} = (ea/(2\hbar\omega))^2[I(V + \hbar\omega/e) - 2I(V) + I(V - \hbar\omega/e)]$. This is physically equivalent to retaining only the contribution of the first two sidebands with $n = \pm 1$ [25]. This simple approximation already shows that P_{int} is indeed reduced by increasing the amplitude a. Furthermore, when the amplitude becomes comparable to the matching peak voltage V_p, the ac signal starts to explore points of the $I(V)$ characteristic curve with positive current ($I > 0$) and the averaged thermocurrent needs to be correspondingly suppressed.

The previous discussion shows that the PAT in general just redistributes the thermoelectric power but does not increase, on average, the intrinsic thermoelectric capabilities of the junction. This is not unexpected, since also for the cooling properties of normal-metal–insulator–superconductor tunnel junctions a similar result is observed for the cooling capabilities in the presence of PAT [53–56]. However, the redistribution due to PAT determines new values of voltages (sidebands) where the system is strongly thermoelectric for biases where the thermoelectric performance was originally smaller. For such particular values of the bias, one observes a microwave *enhanced* bipolar thermoelectricity. Furthermore, in the absence of an ac source, the thermoelectric peaks can be very narrow in voltage range, so a change in the operating point (dc voltage) could result in a drastic reduction of the thermoelectric power. This may happen, for example, with a change in the load resistance when the junction operates as a thermoelectric generator. The ac source widening the $\bar{I}(V)$ characteristic thermoelectric curve reduces the issue of a precise biasing. At the same time, it allows one to tune the voltages where the thermoelectric effect is maximized by varying ω, and in this way it increases the tunability of the device. In other words, there are regimes in the biases where the thermoelectricity is literally microwave-assisted, showing a unique interplay between thermoelectricity and coherent absorption and emission of photons. This increased tunability and better performance at specific biases may be relevant for some specific applications. Furthermore, we expect that the photon detection in S-I-S' junctions can be quantum-limited [36,37], analogously to what has been reported for tunnel junctions in the equilibrium (dissipative) case [24,25].

In Fig. 2 we analyze the power generated by the thermoelectric effect. Figure 2(a) shows the maximum power for a given a and ω, i.e., the point of the $\bar{I}$ characteristic curve which maximizes the thermoelectric power $P = \max_V(-\bar{I}(V)V)$. For low values of a, the maximum power still coincides with the central peak. But increasing the amplitude of the ac source decreases the depth of the central peak, reducing the maximum power accordingly. Above a certain amplitude, roughly delimited by the lower dashed line in Fig. 2(a), the maximum power shows an oscillatory behavior. This dashed line represents the points where the weight of the first terms in the series given by Eq. (2) becomes greater than the zeroth term with increasing amplitude, i.e., $J_1(ea/\hbar\omega) = J_0(ea/\hbar\omega)$ for $ea/\hbar\omega = 1.43$. Therefore, above this line, the maximum power can also be found in one of the sidebands. In the presence of PAT, the power of the sidebands varies significantly with ω, generating this complex oscillatory behavior presented in Fig. 2(a). The middle ($ea/\hbar\omega = 2.63$) and upper ($ea/\hbar\omega = 3.77$) dashed lines correspond to the boundaries where the second ($|n| = 2$) and third ($|n| = 3$) terms, respectively, become predominant in Eq. (2). As shown in Fig. 2(a), there is a shift of the oscillating pattern delimited by the middle dashed line, and the oscillating behavior almost vanishes above the upper line.

In Fig. 2(b) we show the Seebeck voltage V_S dependence on the amplitude a taken at different frequencies ω. It can be seen that V_S increases in steps by increasing the amplitude. As discussed above, the influence of a on the thermoelectric effect is to redistribute the power to other voltages by increasing the number of thermoelectric sideband peaks. Each step is associated with the contribution of additional sidebands which, once they cross the $\bar{I} = 0$ line, shift the Seebeck voltage sharply. However, beyond a certain value of a, as discussed above, the suppression of the thermoelectric effect leads to a drop of the Seebeck voltage, as shown by the $\hbar\omega = 0.06\Delta_{0,1}$ (blue) line.

The S-I-S' junction can be used as a thermoelectric power source by replacing the external dc voltage source

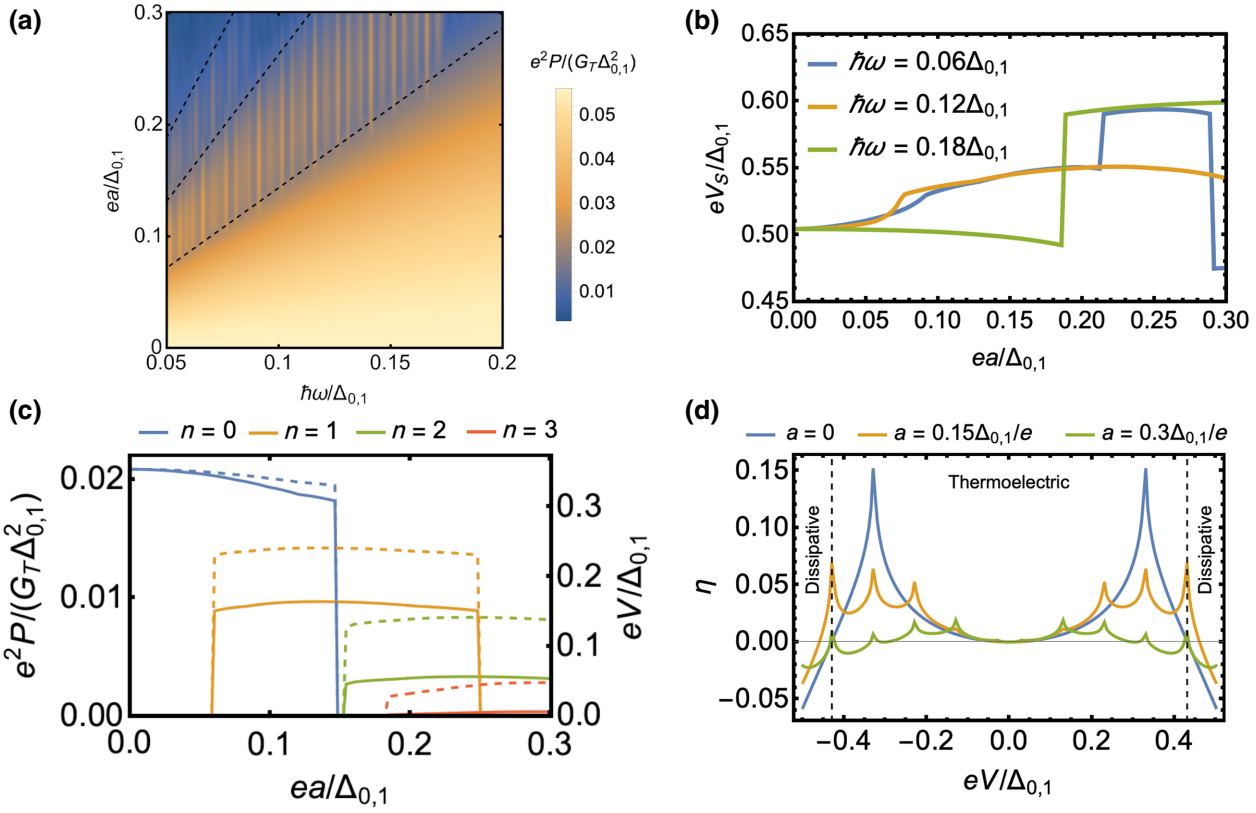

FIG. 2. (a) Maximum power and (b) Seebeck voltage as functions of the amplitude and angular frequency of the ac field. (c) Power (solid) and voltage (dashed) of the stable points of the $\bar{I}(V)$ characteristic curve for a fixed load $R = 6G_T^{-1}$. (d) Efficiency η of the thermoelectric effect. In panels (c) and (d), the frequency is set to $\hbar\omega = 0.1\Delta_{0,1}$. The temperatures of the superconducting electrodes are $T_1 = 0.7T_{c,1}$ and $T_2 = 0$ for panels (a), (c), and (d), and $T_1 = 0.6T_{c,1}$ and $T_2 = 0$ for panel (b).

with a resistive load R. Ohm's law constrains the values that the current and the voltage can take, so that the current can only flow when the junction operates as a thermoelectric generator. The operating points are determined by the intersection of the $\bar{I}(V)$ characteristic curve with a line of slope $-1/R$. Similarly to the purely dc case, only the solutions with a *positive* $d\bar{I}/dV$ are stable in the presence of PAT [15,16,18]. As shown in Fig. 2(c), the inclusion of an ac voltage source allows also for multiple stable working points which appear at different voltages (dashed lines) and consequently different powers (solid lines). In the example, we consider a load value of $R = 6G_T^{-1}$. For certain ac amplitudes we get multiple stable points labeled with different n. The $n = 0$ (blue) line corresponds to the solution associated with the matching peak, while the $n = 1, 2, 3$ lines correspond to sidebands with a lower voltage. It is possible to find stable points with a higher voltage by choosing a higher load resistance (not shown). For $0.06 < ea/\Delta_{0,1} < 0.15$, one can find two stable working points for $n = 0$ (blue), due to the main peak, and $n = 1$ (yellow), corresponding to the first sideband. The system can be driven to the stable working points by applying current pulses similarly to what has been realized in Ref. [18] in the absence of any ac signal. Therefore, PAT can be used to design devices with an increased number of states occurring at different voltages. This, for example, would increase the number of logic states of the proposed thermoelectric volatile memory [57–59].

Figure 2(d) shows the thermal efficiency $\eta = \dot{W}/\dot{Q}_1$, which describes the ratio of the net work output to the heat input, for different values of a. As in the case of the power, the inclusion of an ac source does not offer a way to increase globally the maximum efficiency. However, the widening of the curves is beneficial to avoid efficiency drops stemming from changes in the voltage operating point. The dashed vertical lines in Fig. 2(d) show the area where the system is thermoelectric $V < V_S$, and where it is dissipative in the absence of the ac signal. We see that PAT *widens* the voltage values where the system is thermoelectric. The ac signal leads to a moderate efficiency reduction at the matching peak, but it increases its efficiency for certain values of V.

Finally, in Fig. 3 we investigate the cooling power of the S-I-S' junction. By applying an external bias, for specific temperature conditions [16], it is possible to extract heat and reduce the electronic temperature of the lower-gap

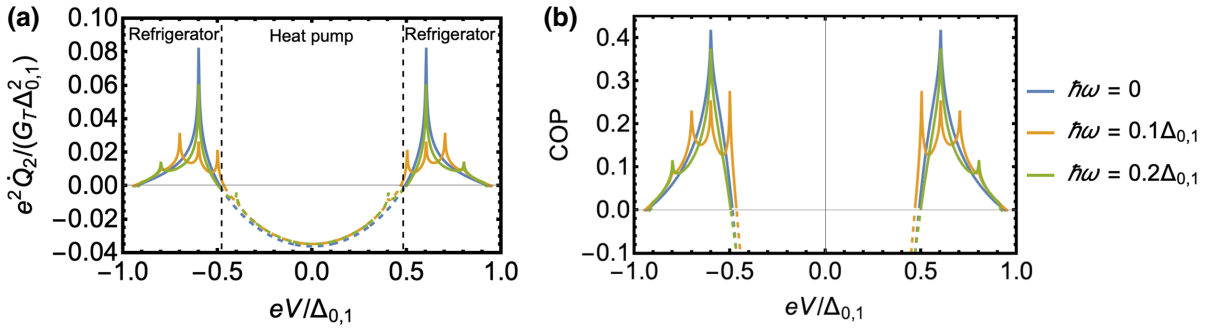

FIG. 3. (a) Heat current (cooling power) extracted from the right (cold) superconducting electrode in the cooling regime and (b) coefficient of performance (COP) for different frequencies. The amplitude of the ac voltage is set to $ea = 0.15\Delta_{0,1}$. The temperatures of the superconducting electrodes are $T_1 = 0.5T_{c,1}$ and $T_2 = 0.4T_{c,1}$.

superconductor [16,43,54]. In Fig. 3(a) we show the heat extracted from the lower-gap superconductor for temperatures $T_1 = 0.5T_{c,1}$ and $T_2 = 0.4T_{c,1}$. The voltage range where there is no cooling is represented by dashed lines. If the applied voltage is small, the system does not reach the cooling regime and the heat flows from the hot to the cold terminal. The cooling shares some similarities with the thermoelectric effect; it requires the hot superconductor to possess a larger gap than the cold superconductor and the cooling power is maximized at voltage bias $eV = \Delta_1 - \Delta_2$. With PAT, the ac voltage source creates additional sidebands to the cooler, *widening* the window where the cooling is possible [53]. Figure 3(b) shows the coefficient of performance $\mathrm{COP} = -\dot{Q}_2/\dot{W}$, which describes the efficiency of the extracted heat with respect to the applied work. Similarly to the thermoelectric efficiency, the maximum COP is slightly suppressed by the presence of PAT since also in this case the PAT will not increase globally the efficiency of the system but will redistribute the cooling capabilities over different cooling sidebands. Analogously to the thermoelectricity, there are specific values of the bias where the cooling is microwave-enhanced.

IV. CONCLUSIONS

In this work, we have discussed the influence of photon-assisted tunneling on the bipolar thermoelectric effect occurring in an S-I-S' tunnel junction. The ac voltage source leads to a weighted replication of the bipolar thermoelectric dc characteristic curve displaced in voltages. This leads to the appearance of sidebands whose position is determined by the frequency of the ac field. The redistribution of the power to other voltages leads globally to a reduction of the net thermopower output of the matching peak, but it broadens the thermoelectric region, potentially increasing even the obtainable Seebeck voltage. Therefore, changes in the operating point of the junction will have a less dramatic effect over the thermoelectric performance. We have specifically investigated how this redistribution mechanism of the bipolar thermoelectricity is influenced by the ac signal amplitude. The photon emission and absorption sidebands for the bipolar thermoelectricity constitute, in a certain sense, *microwave-assisted thermoelectricity*. The thermoelectric power and the efficiency for some specific values of the voltages is even enhanced.

Furthermore, the system can be driven to the additional stable working points selected by the sidebands, so PAT can be used to design devices with an increased number of states at different voltages, potentially increasing the number of logic states of a thermoelectric volatile memory [57–59].

Finally, we have studied the influence of PAT on the cooling performance of the junction. Similar to the thermoelectric effect, the cooling power is also influenced by the presence of PAT, and the redistribution of the cooling capabilities into sidebands also allows one to increase the COP at specific voltages.

From the fundamental point of view, this application shows the intriguing interplay between thermoelectricity and coherent photon absorption and emission in an experimentally accessible setup. We think that the obtained results could be relevant for quantum-limited microwave detection [18,19], quantum sensing, and microwave-superconducting technologies.

ACKNOWLEDGMENTS

A.H. acknowledges funding from the University of the Basque Country (Project PIF20/05). F.S.B. acknowledges financial support from Spanish AEI through projects PID2020-114252GB-I00 (SPIRIT) and TED2021-130292B-C42, the Basque Government through Grant No. IT-1591-22, and the A. v. Humboldt Foundation. F.S.B. and F.G. acknowledge the EU Horizon 2020 Research and Innovation Framework Programme under Grant No. 800923 (SUPERTED). F.G. and A.B. acknowledge the EU Horizon 2020 Research and Innovation Framework Programme under Grants No. 964398 (SUPERGATE) and No. 101057977 (SPECTRUM). A.B.

acknowledges the Royal Society through the International Exchanges between the UK and Italy (Grants No. IEC R2 192166 and No. IEC R2 212041).

[1] F. S. Bergeret, M. Silaev, P. Virtanen, and T. T. Heikkilä, Colloquium: Nonequilibrium effects in superconductors with a spin-splitting field, Rev. Mod. Phys. **90**, 041001 (2018).

[2] T. T. Heikkilä, M. Silaev, P. Virtanen, and F. S. Bergeret, Thermal, electric and spin transport in superconductor/ferromagnetic-insulator structures, Prog. Surf. Sci. **94**, 100540 (2019).

[3] P. Machon, M. Eschrig, and W. Belzig, Nonlocal Thermoelectric Effects and Nonlocal Onsager Relations in a Three-Terminal Proximity-Coupled Superconductor-Ferromagnet Device, Phys. Rev. Lett. **110**, 047002 (2013).

[4] A. Ozaeta, P. Virtanen, F. Bergeret, and T. Heikkilä, Predicted Very Large Thermoelectric Effect in Ferromagnet-Superconductor Junctions in the Presence of a Spin-Splitting Magnetic Field, Phys. Rev. Lett. **112**, 057001 (2014).

[5] S. Kolenda, M. J. Wolf, and D. Beckmann, Observation of Thermoelectric Currents in High-Field Superconductor-Ferromagnet Tunnel Junctions, Phys. Rev. Lett. **116**, 097001 (2016).

[6] T. T. Heikkilä, R. Ojajärvi, I. J. Maasilta, E. Strambini, F. Giazotto, and F. S. Bergeret, Thermoelectric Radiation Detector based on Superconductor-Ferromagnet Systems, Phys. Rev. Appl. **10**, 034053 (2018).

[7] S. Chakraborty and T. T. Heikkilä, Thermoelectric radiation detector based on a superconductor-ferromagnet junction: Calorimetric regime, J. Appl. Phys. **124**, 123902 (2018).

[8] E. Strambini, M. Spies, N. Ligato, S. Ilić, M. Rouco, C. González-Orellana, M. Ilyn, C. Rogero, F. Bergeret, J. Moodera, *et al.*, Superconducting spintronic tunnel diode, Nat. Commun. **13**, 1 (2022).

[9] Z. Geng and I. J. Maasilta, Analytical models for the pulse shape of a superconductor-ferromagnet tunnel junction thermoelectric microcalorimeter, J. Low Temp. Phys. **209**, 419 (2022).

[10] R. Meservey and P. Tedrow, Spin-polarized electron tunneling, Phys. Rep. **238**, 173 (1994).

[11] J. S. Moodera, T. S. Santos, and T. Nagahama, The phenomena of spin-filter tunnelling, J. Phys.: Condens. Matter **19**, 165202 (2007).

[12] G.-X. Miao, J. Chang, B. A. Assaf, D. Heiman, and J. S. Moodera, Spin regulation in composite spin-filter barrier devices, Nat. Commun. **5**, 3682 (2014).

[13] G. De Simoni, E. Strambini, J. S. Moodera, F. S. Bergeret, and F. Giazotto, Toward the absolute spin-valve effect in superconducting tunnel junctions, Nano Lett. **18**, 6369 (2018).

[14] J. P. Morten, A. Brataas, and W. Belzig, Spin transport and magnetoresistance in ferromagnet/superconductor/ferromagnet spin valves, Phys. Rev. B **72**, 014510 (2005).

[15] G. Marchegiani, A. Braggio, and F. Giazotto, Nonlinear Thermoelectricity with Electron-Hole Symmetric Systems, Phys. Rev. Lett. **124**, 106801 (2020).

[16] G. Marchegiani, A. Braggio, and F. Giazotto, Superconducting nonlinear thermoelectric heat engine, Phys. Rev. B **101**, 214509 (2020).

[17] G. Marchegiani, A. Braggio, and F. Giazotto, Phase-tunable thermoelectricity in a Josephson junction, Phys. Rev. Res. **2**, 043091 (2020).

[18] G. Germanese, F. Paolucci, G. Marchegiani, A. Braggio, and F. Giazotto, Bipolar thermoelectric Josephson engine, Nat. Nanotechnol. **17**, 1084 (2022).

[19] G. Germanese, F. Paolucci, G. Marchegiani, A. Braggio, and F. Giazotto, Phase Control of Bipolar Thermoelectricity in Josephson Tunnel Junctions, Phys. Rev. Appl. **19**, 014074 (2023).

[20] P. K. Tien and J. P. Gordon, Multiphoton process observed in the interaction of microwave fields with the tunneling between superconductor films, Phys. Rev. **129**, 647 (1963).

[21] J. N. Sweet and G. I. Rochlin, Microwave-photon-assisted tunneling in Sn-I-Sn superconducting tunnel junctions, Phys. Rev. B **2**, 656 (1970).

[22] C. A. Hamilton and S. Shapiro, rf-induced effects in superconducting tunnel junctions, Phys. Rev. B **2**, 4494 (1970).

[23] B. Kofoed, U. K. Poulsen, and K. Saermark, Microwave-assisted tunnelling effects in small-area thin-film superconducting tunnel junctions, Phys. Status Solidi A **23**, 87 (1974).

[24] J. Tucker, Quantum limited detection in tunnel junction mixers, IEEE J. Quantum Electron. **15**, 1234 (1979).

[25] J. R. Tucker and M. J. Feldman, Quantum detection at millimeter wavelengths, Rev. Mod. Phys. **57**, 1055 (1985).

[26] K. Hamasaki, K. Yoshida, F. Irie, and K. Enpuku, Capacitance measurement of Josephson tunnel junctions with microwave-induced dc quasiparticle tunneling currents, J. Appl. Phys. **53**, 3713 (1982).

[27] S. P. Kashinje and P. Wyder, Photon-assisted tunnelling in a magnetic field, J. Phys. C: Solid State Phys. **19**, 3193 (1986).

[28] Q.-f. Sun, J. Wang, and T.-h. Lin, Photon-assisted Andreev tunneling through a mesoscopic hybrid system, Phys. Rev. B **59**, 13126 (1999).

[29] B. Leone, J. Gao, T. Klapwijk, B. Jackson, W. Laauwen, and G. de Lange, Hot electron effect in terahertz hybrid devices, IEEE Trans. Appl. Supercond. **11**, 649 (2001).

[30] P. Kot, R. Drost, M. Uhl, J. Ankerhold, J. C. Cuevas, and C. R. Ast, Microwave-assisted tunneling and interference effects in superconducting junctions under fast driving signals, Phys. Rev. B **101**, 134507 (2020).

[31] M. Houzet, K. Serniak, G. Catelani, M. H. Devoret, and L. I. Glazman, Photon-Assisted Charge-Parity Jumps in a Superconducting Qubit, Phys. Rev. Lett. **123**, 107704 (2019).

[32] X. Pan, Y. Zhou, H. Yuan, L. Nie, W. Wei, L. Zhang, J. Li, S. Liu, Z. H. Jiang, G. Catelani, L. Hu, F. Yan, and D. Yu, Engineering superconducting qubits to reduce quasiparticles and charge noise, Nat. Commun. **13**, 7196 (2022).

[33] C.-H. Liu, D. C. Harrison, S. Patel, C. D. Wilen, O. Rafferty, A. Shearrow, A. Ballard, V. Iaia, J. Ku, B. L. T. Plourde, and R. McDermott, Quasiparticle poisoning of superconducting qubits from resonant absorption of pair-breaking photons, ArXiv:2203.06577 (2022)

[34] S. Diamond, V. Fatemi, M. Hays, H. Nho, P. D. Kurilovich, T. Connolly, V. R. Joshi, K. Serniak, L. Frunzio, L. I. Glazman, and M. H. Devoret, Distinguishing Parity-Switching Mechanisms in a Superconducting Qubit, PRX Quantum **3**, 040304 (2022).

[35] G. Marchegiani, L. Amico, and G. Catelani, Quasiparticles in Superconducting Qubits with Asymmetric Junctions, PRX Quantum **3**, 040338 (2022).

[36] F. Paolucci, G. Germanese, A. Braggio, and F. Giazotto, A highly-sensitive broadband superconducting thermoelectric single-photon detector, ArXiv:2302.02933 (2023)

[37] G. Germanese, F. Paolucci, A. Braggio, and F. Giazotto, Broadband passive superconducting thermoelectric single-photon detector, Patent (06/02/2023), Filing number: 102023000001854.

[38] A. Barone and G. Paternò, *Physics and Applications of the Josephson Effect* (Wiley, New York, 1982), p. 35. (Chapter 2)

[39] B. Josephson, Possible new effects in superconductive tunnelling, Phys. Lett. **1**, 251 (1962).

[40] R. E. Harris, Cosine and other terms in the Josephson tunneling current, Phys. Rev. B **10**, 84 (1974).

[41] D. R. Gulevich, V. P. Koshelets, and F. V. Kusmartsev, Josephson flux-flow oscillator: The microscopic tunneling approach, Phys. Rev. B **96**, 024515 (2017).

[42] A. Barone, G. Paternò, M. Russo, and R. Vaglio, Light-induced transition from "small" to "large" Josephson junctions, Phys. Lett. A **53**, 393 (1975).

[43] F. Giazotto, T. T. Heikkilä, A. Luukanen, A. M. Savin, and J. P. Pekola, Opportunities for mesoscopics in thermometry and refrigeration: Physics and applications, Rev. Mod. Phys. **78**, 217 (2006).

[44] A. Fornieri and F. Giazotto, Towards phase-coherent caloritronics in superconducting circuits, Nat. Nanotechnol. **12**, 944 (2017).

[45] R. C. Dynes, V. Narayanamurti, and J. P. Garno, Direct Measurement of Quasiparticle-Lifetime Broadening in a Strong-Coupled Superconductor, Phys. Rev. Lett. **41**, 1509 (1978).

[46] F. Giazotto, T. T. Heikkilä, F. Taddei, R. Fazio, J. P. Pekola, and F. Beltram, Tailoring Josephson Coupling through Superconductivity-Induced Nonequilibrium, Phys. Rev. Lett. **92**, 137001 (2004).

[47] A. V. Timofeev, C. P. García, N. B. Kopnin, A. M. Savin, M. Meschke, F. Giazotto, and J. P. Pekola, Recombination-Limited Energy Relaxation in a Bardeen-Cooper-Schrieffer Superconductor, Phys. Rev. Lett. **102**, 017003 (2009).

[48] M. J. Martínez-Pérez, A. Fornieri, and F. Giazotto, Rectification of electronic heat current by a hybrid thermal diode, Nat. Nanotechnol. **10**, 303 (2015).

[49] J. K. Julin, S. Chaudhuri, M. Laitinen, T. Sajavaara, and I. J. Maasilta, Stability, sub-gap current, 1/f-noise, and elemental depth profiling of annealed Al:Mn-AlO_x-Al normal metal-insulator-superconducting tunnel junctions, AIP Adv. **6**, 125026 (2016).

[50] G. Falci, V. Bubanja, and G. Schön, Quasiparticle and Cooper pair tenneling in small capacitance Josephson junctions, Z. Phys. B Condens. Matter **85**, 451 (1991).

[51] N. S. Wingreen, A.-P. Jauho, and Y. Meir, Time-dependent transport through a mesoscopic structure, Phys. Rev. B **48**, 8487 (1993).

[52] A.-P. Jauho, N. S. Wingreen, and Y. Meir, Time-dependent transport in interacting and noninteracting resonant-tunneling systems, Phys. Rev. B **50**, 5528 (1994).

[53] N. B. Kopnin, F. Taddei, J. P. Pekola, and F. Giazotto, Influence of photon-assisted tunneling on heat flow in a normal metal-superconductor tunnel junction, Phys. Rev. B **77**, 104517 (2008).

[54] J. T. Muhonen, M. Meschke, and J. P. Pekola, Micrometre-scale refrigerators, Rep. Prog. Phys. **75**, 046501 (2012).

[55] K. Y. Tan, M. Partanen, R. E. Lake, J. Govenius, S. Masuda, and M. Möttönen, Quantum-circuit refrigerator, Nat. Commun. **8**, 15189 (2017).

[56] M. Silveri, H. Grabert, S. Masuda, K. Y. Tan, and M. Möttönen, Theory of quantum-circuit refrigeration by photon-assisted electron tunneling, Phys. Rev. B **96**, 094524 (2017).

[57] F. Giazotto, F. Paolucci, A. Braggio, G. Marchegiani, and G. Germanese, Superconducting bipolar thermoelectric memory and method for writing a superconducting bipolar thermoelectric memory, Patent (21/12/2021), Filing number: 102021000032042.

[58] G. Marchegiani, A. Braggio, and F. Giazotto, Noise effects in the nonlinear thermoelectricity of a Josephson junction, Appl. Phys. Lett. **117**, 212601 (2020).

[59] C. Guarcello, P. Solinas, A. Braggio, M. Di Ventra, and F. Giazotto, Josephson Thermal Memory, Phys. Rev. Appl. **9**, 014021 (2018).